

# Non-thermal radio emission from O-type stars

## V. 9 Sgr

R. Blomme and D. Volpi

Royal Observatory of Belgium, Ringlaan 3, B-1180 Brussel, Belgium  
e-mail: Ronny.Blomme@oma.be

Received date; accepted date

### ABSTRACT

*Context.* The colliding winds in a massive binary system generate synchrotron emission due to a fraction of electrons that have been accelerated to relativistic speeds around the shocks in the colliding-wind region.

*Aims.* We studied the radio light curve of 9 Sgr = HD 164794, a massive O-type binary with a 9.1-yr period. We investigated whether the radio emission varies consistently with orbital phase and we determined some parameters of the colliding-wind region.

*Methods.* We reduced a large set of archive data from the Very Large Array (VLA) to determine the radio light curve of 9 Sgr at 2, 3.6, 6 and 20 cm. We also constructed a simple model that solves the radiative transfer in the colliding-wind region and both stellar winds.

*Results.* The 2-cm radio flux shows clear phase-locked variability with the orbit. The behaviour at other wavelengths is less clear, mainly due to a lack of observations centred on 9 Sgr around periastron passage. The high fluxes and nearly flat spectral shape of the radio emission show that synchrotron radiation dominates the radio light curve at all orbital phases. The model provides a good fit to the 2-cm observations, allowing us to estimate that the brightness temperature of the synchrotron radiation emitted in the colliding-wind region at 2 cm is at least  $4 \times 10^8$  K.

*Conclusions.* The simple model used here already allows us to derive important information about the colliding-wind region. We propose that 9 Sgr is a good candidate for more detailed modelling, as the colliding-wind region remains adiabatic during the whole orbit thus simplifying the hydrodynamics.

**Key words.** stars: individual: HD 164794 - stars: early-type - stars: mass-loss - radiation mechanisms: non-thermal - acceleration of particles - radio continuum: stars

## 1. Introduction

In a massive-star binary the stellar winds collide, forming two shocks, one on each side of the contact discontinuity. In this colliding-wind region (CWR) the material gets heated and compressed (Eichler & Usov 1993). If the binary has a sufficiently long period, the time scale for radiative cooling of the material will far exceed the flow time scale, and the CWR will not be able to cool down. The CWR is thus in the adiabatic regime. The high temperature leads to an excess of X-ray emission, which also has a harder spectrum than the X-ray contribution of the stellar winds themselves (Stevens et al. 1992; Gagné et al. 2012).

The CWR also has an important effect on the radio continuum emission. Around the shocks, the Fermi mechanism accelerates a fraction of the electrons up to relativistic speeds (Eichler & Usov 1993). These electrons then emit synchrotron radiation as they spiral in the magnetic field. This synchrotron radiation can be detected at radio wavelengths. It can be recognized by an excess flux compared to that expected from the free-free wind emission, by variability that is locked to the orbital phase, by a high brightness temperature, and by a non-thermal spectral index<sup>1</sup> (Bieging et al. 1989). Bieging et al. consider a spectral index  $\alpha < 0.0$  to be a clear indicator of non-thermal emission, as it is significantly different from the  $\alpha = +0.6$  expected for thermal emission in a spherically symmetric stellar wind.

Previous papers in this series have studied a number of these non-thermal radio emitters. For HD 168112, we found that the radio fluxes show periodic behaviour, suggesting that it is a binary system, though this still awaits confirmation by spectroscopic observations (Blomme et al. 2005). For Cyg OB2 #9, we also detected periodic behaviour in the radio fluxes (Van Loo et al. 2008), while Nazé et al. (2008) used spectroscopic observations to show the binary nature of this system. Later, we monitored the periastron passage of Cyg OB2 #9 in detail, allowing us to model the system (Nazé et al. 2012; Blomme et al. 2013). For Cyg OB2 #8A (a known binary) we showed that the radio data are better explained by assuming the secondary component to have the stronger wind (Blomme et al. 2010). The radio variability of HD 167971 (a triple system) suggests that we are detecting the CWR between the binary at the core of the system and the third component further away (Blomme et al. 2007).

In this paper, we study 9 Sgr = HD 164794. Proof that 9 Sgr is a binary was a long time coming. This allowed for the possibility that the non-thermal radio emission was somehow intrinsic to the stellar wind of 9 Sgr itself. In a single star, the shocks due to the intrinsic instability of the radiation driving mechanism would be the sites where the Fermi acceleration mechanism operates (White 1985). However, Van Loo et al. (2006) showed that single-star winds are unlikely to explain the non-thermal radio emission.

First hints of the binary nature of 9 Sgr came from the excess of X-ray emission and the long-term radial velocity variations in

<sup>1</sup> The spectral index is the quantity  $\alpha$  in  $F_\nu \propto \nu^\alpha$ .

the optical spectra (Rauw et al. 2002). Later, Rauw et al. (2005) showed 9 Sgr to have a clear SB2 signature, but the period could only be estimated. Finally, Rauw et al. (2012) showed that 9 Sgr is a spectroscopic binary, with an O3.5 V((f<sup>+</sup>)) primary and an O5–5.5 V((f)) secondary. It has a highly eccentric orbit ( $e = 0.7$ ) with a period that Rauw et al. determined to be 8.6 years, but which has recently been revised to 9.1 year (Rauw, 2013, pers. comm.). The long period of this system explains why it was so difficult to prove the binarity.

Among the O+O binaries, 9 Sgr is the system with the longest known period. A study of its colliding-wind region is therefore important as it samples a significantly different part of the parameter space of colliding-wind binaries.

Abbott et al. (1980) were the first to detect 9 Sgr at radio wavelengths. Their flux value, interpreted in a strictly thermal wind model, led to a radio mass-loss rate a factor 40 higher than that from H $\alpha$  and the ultraviolet P Cygni profiles. A second observation showed some possible variability (Abbott et al. 1981). Further monitoring allowed Abbott et al. (1984) to conclude that 9 Sgr is a non-thermal radio emitter, because of the non-thermal spectral index and the flux variability. This was confirmed by additional data by Bieging et al. (1989). A clear non-thermal spectral index was also found in the radio data analysed by Rauw et al. (2002). They modelled the radio observations under the then current assumption that the star was single.

In this paper, we use data from the Very Large Array (VLA) archive to study the radio light curve of 9 Sgr. In Sect. 2 we present the data and their reduction. We discuss the resulting radio light curve in Sect. 3. In Sect. 4 we present the model for the colliding-wind region which we used to interpret the observations. We discuss the results of this modelling in Sect. 5, and we present our conclusions in Sect. 6.

## 2. Data reduction

We selected all data from the VLA archive that were centred on, or close to, 9 Sgr. The data found cover a range of 24 years. We reduced the visibility data using the Astronomical Image Processing System (AIPS), developed by the NRAO. We applied the standard procedures for antenna gain calibration, absolute flux calibration, imaging and deconvolution. The absolute flux calibration uses a model for the flux calibrator when that is available. For details of the data reduction, we refer to the previous papers in this series (Blomme et al. 2005, 2007; Van Loo et al. 2008; Blomme et al. 2010).

When the VLA is in one of the configurations with lower spatial resolution, the resulting images are dominated by the presence of the Hourglass Nebula. This is a blister-type H II region ionized by the O7.5 V star Herschel 36 (Kumar & Anandarao 2010). It is a much stronger radio source than 9 Sgr itself. At 6 cm, in the configuration with the lowest spatial resolution, the flux of the Hourglass Nebula is 0.7 – 1.7 Jy (depending on the exact configuration). At 20 cm, the flux is 3.6 – 4.3 Jy. This is to be compared to the 9 Sgr flux which is of order 1 – 10 mJy. The problem with the high Hourglass Nebula flux does not occur at higher spatial resolutions because of the filtering properties of a radio interferometer: the 6-cm flux is only  $\sim 5$  mJy and the 20 cm one 20 – 30 mJy for the configuration with the highest spatial resolution.

The high flux of the Hourglass Nebula considerably complicates the detection of 9 Sgr and the measurement of its flux. We therefore modelled this source separately and then subtracted it directly from the visibility data. Further background is removed

by systematically dropping visibility data on the shortest baselines. In this way, we typically achieve a 1-sigma noise level of 2 – 10 mJy at 6 cm and 30 – 50 mJy at 20 cm for the configurations with the lowest spatial resolution, but these values are still too high to allow a detection. It is only at the higher spatial resolution configurations that we can detect 9 Sgr. For those data sets where 9 Sgr is detected, we further applied a single round of phase-only self-calibration.

We measured the fluxes and error bars by fitting an elliptical Gaussian to the source on the images. The results are listed in the Appendix in Table A.1. The error bars include not only the rms noise in the map, but also an estimate of the systematic errors that were evaluated using a jack-knife technique. This technique drops part of the observed data and re-determines the fluxes, giving some indication of systematic errors that are present. Note that the absolute calibration uncertainty is not included in the error bars listed in the table. These uncertainties are estimated at 1–2 % at 20, 6, and 3.6 cm, and 3–5 % at 2 and 0.7 cm (Perley & Taylor 2003). Where the source could not be detected, we assigned an upper limit of three times the rms noise around the measured position.

A number of observations are not centred on 9 Sgr, but on another, nearby, target. The 9 Sgr flux values and error bars for these observations have been corrected for the decreasing sensitivity of the primary beam and for the increased size a point source has due to bandwidth smearing (Bridle & Schwab 1999). As the bandwidth smearing effect spreads out the flux over a larger area, the flux measurement becomes more difficult and the values should therefore be considered as less reliable.

When there are multiple targets for one observation, we list in Table A.1 only that one with the best detection or the lowest noise level (in case of a non-detection). This is usually the one where the field centre is closest to 9 Sgr. The exceptions are the two AF399 3.6-cm observations, where the integration time on the offset position is much longer than on 9 Sgr, resulting in a better image. We further exclude from Table A.1 those observations with upper limits higher than 50 mJy (which corresponds to about 4 times the highest detection at all wavelengths).

To further increase the signal, we also combined data that were taken close-by in time. This procedure of course assumes that there are no significant changes on short timescales. As we are looking for variability related to the 9.1-year orbital period, we combined data that were taken less than 1 month apart.

Table 1 shows a comparison with values previously published in the literature. Our current values of the AB1005 3.6 and 20-cm fluxes are very different from those of our previous reduction of the same data given in Rauw et al. (2002). In that paper, we used the less sophisticated technique of removing data on short and intermediate-length baselines to remove the effect of the Hourglass nebula. Our current technique of subtracting the Hourglass nebula visibilities from the original data is better adapted to handle the problem of this strong, nearby source. The flux values presented here therefore supersede those published in Rauw et al.

Bieging et al. (1989) list a number of flux determinations based on data in common with those discussed here. The major difference found is in the CHUR (1979-07-13) 6 cm flux. Bieging et al. give a value of  $1.0 \pm 0.4$  mJy, while we find  $9.0 \pm 2.7$  mJy. Details of their data reduction are given in Abbott et al. (1980), who point out the problems in the data reduction due to the presence of M 8 (or, more correctly, the Hourglass nebula). Apparently, the procedure they used to remove the effect of the nebula is not based on subtracting the Hourglass nebula visibilities. We therefore have greater confidence in the re-

**Table 1.** Comparison of our radio fluxes with those in the literature.

ID	date	literature flux (mJy)	our flux (mJy)	ref
<b>2 cm</b>				
BIEG	1982-02-09	<2.4	<2	1
AC42	1983-08-22	<0.8	<0.9	1
AC116	1985-02-16	$0.7 \pm 0.1$	$1.01 \pm 0.28$	1
<b>3.6 cm</b>				
AB1005	2001-03-08	$1.6 \pm 0.4$	$3.6 \pm 0.9$	2
<b>6 cm</b>				
CHUR	1979-07-13	$1.0 \pm 0.4$	$9.0 \pm 2.7$	1
CHUR	1980-05-22	$1.8 \pm 0.3$	$1.82 \pm 0.47$	1
BIEG	1982-02-09	$2.5 \pm 0.3$	$1.70 \pm 0.28$	1
BIGN	1982-05-26	$2.4 \pm 0.3$	$2.76 \pm 0.11$	1
AC42	1983-08-22	$1.5 \pm 0.2$	$2.20 \pm 0.14$	1
AC116	1984-11-27	$2.0 \pm 0.2$	$1.94 \pm 0.22$	1
AB327	1985-01-28	$1.5 \pm 0.1$	$2.08 \pm 0.19$	1
AC116	1985-02-16	$1.9 \pm 0.1$	$1.96 \pm 0.13$	1
AB1005	2001-03-08	$2.8 \pm 0.4$	$2.9 \pm 0.74$	2
<b>20 cm</b>				
BIGN	1982-05-26	$3.6 \pm 0.3$	$5.23 \pm 0.20$	1
AC42	1983-08-22	$3.9 \pm 0.4$	$3.24 \pm 0.37$	1
AB1005	2001-03-08	$4.5 \pm 1.2$	$12.7 \pm 3.6$	2

**References.** (1) Bieging et al. (1989); (2) Rauw et al. (2002).

sults presented here. Other differences between our results and those of Bieging et al. are smaller, or not significant. We again attribute any significant differences to the different techniques to remove the effect of the Hourglass nebula.

### 3. Radio light curve

We first tried to determine a period from our radio data, using the string-length method (Dworetzky 1983). We normalized the fluxes to their maximum value, so that the flux differences and phase differences have an equal weight. We tried the string-length method with various possibilities: using data at all wavelengths, or only the 6-cm data (as most of our data are at 6 cm), including the observations where 9 Sgr was off-centre, or not. No combination however leads to a period near that of the spectroscopically determined one. As the quality of the spectroscopic data is much better than the radio data we have, from hereon we use the 9.1-year period as determined by Rauw (2013, pers. comm.). Note that this value for the period updates the one given by Rauw et al. (2012).

Figure 1 plots the observed radio fluxes at 2, 3.6, 6 and 20 cm, as a function of phase in the 9.1-year orbit. The 2-cm fluxes clearly show variability: around periastron ( $\pm 0.2$  in phase) the fluxes are high (around 3 mJy), but in the phases in between the fluxes are only 1–2 mJy. For 6 cm, observations centred on 9 Sgr at periastron are lacking. Based on the off-centre data (which are less reliable), there is a suggestion that the fluxes around periastron are high. Away from periastron the fluxes are consistently low (about 2 mJy). For 3.6 cm the picture is less clear: there is also variability, but there is no clear indication of a flux increase near periastron. For 20 cm, the only high flux value is quite some distance away from periastron, and it is surrounded on each side by a lower-flux observation. Other wavelengths (0.7 and 90 cm) have only a single observation with a high upper limit.

The 2-cm behaviour is qualitatively in agreement with what is expected for an eccentric long-period binary. At all orbital

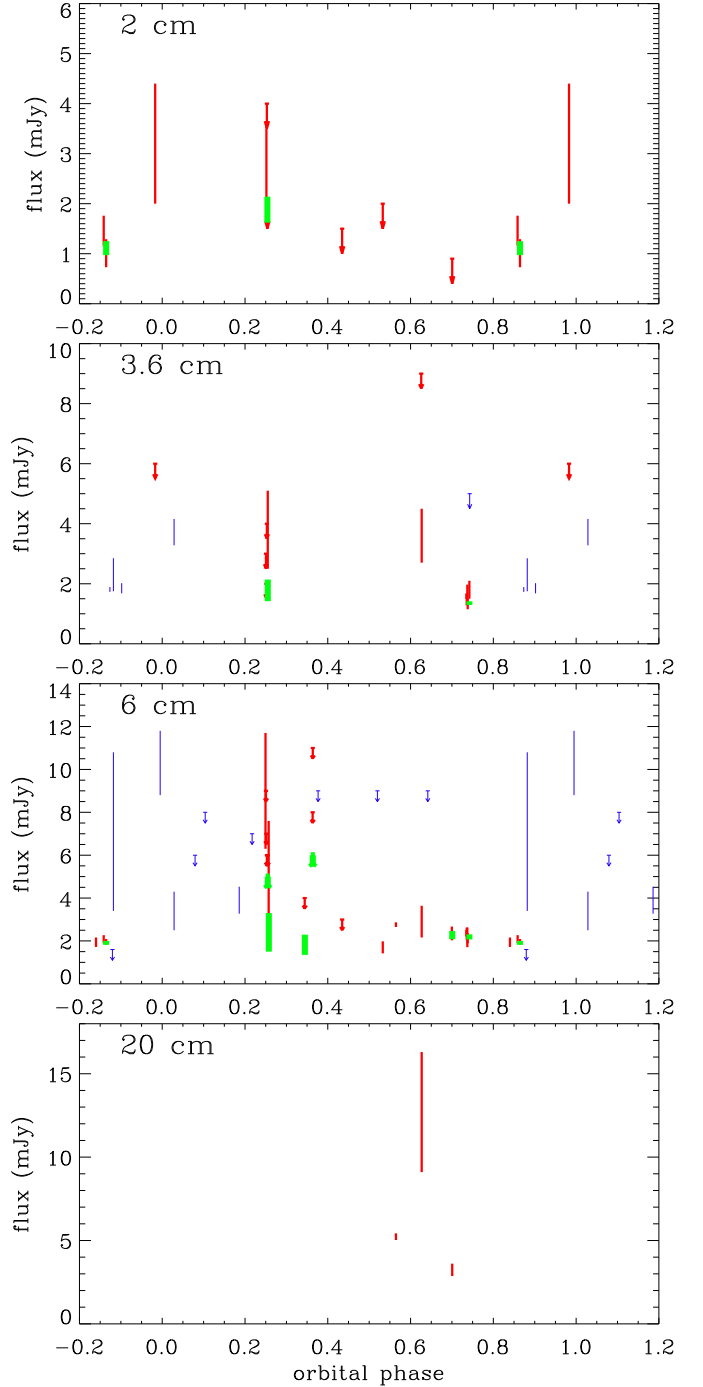


**Fig. 1.** 9 Sgr radio fluxes as a function of orbital phase in the 9.1-year period. The detections are shown with their error bars, the upper limits as arrows. Red data points are observations that are centred on 9 Sgr, blue data points have 9 Sgr off-centre. The green bars indicate data that have been combined. Phase 0.0 corresponds to periastron passage.

phases the stellar winds collide, leading to the generation of synchrotron emission. As the system approaches periastron, the stars move much closer together, leading to a more energetic collision and therefore more synchrotron emission. In principle, this synchrotron emission could be partially or completely absorbed by the free-free absorption of the material in the stellar winds. However, because of the long period of this system, the

**Table 2.** Parameters of 9 Sgr used in this study.

Parameter	symbol	primary	secondary
orbital period	$P$ (d)		3327
time periastron passage	$T_0$ (JD)		2 446 564
eccentricity	$e$	0.702 ± 0.010	
longitude of periastron	$\omega$ (°)	27.4 ± 1.2	
major axis	$a \sin i$ ( $R_\odot$ )	3011	
mass	$m \sin^3 i$ ( $M_\odot$ )	20.0	13.3
mass-loss rate	$\dot{M}$ ( $M_\odot \text{ yr}^{-1}$ )	$9.0 \times 10^{-7}$	$5.0 \times 10^{-7}$
terminal velocity	$v_\infty$ ( $\text{km s}^{-1}$ )	3500	3100
distance	$D$ (kpc)		1.79
estimated inclination	$i$ (°)	45	
thermal flux at 2 cm	$F_{\nu,2}$ (mJy)	0.014	0.007
thermal flux at 6 cm	$F_{\nu,6}$ (mJy)	0.007	0.004
thermal flux at 20 cm	$F_{\nu,20}$ (mJy)	0.003	0.002
effective radius, 2 cm	$R_{\text{eff},2}$ ( $R_\odot$ )	260	190
effective radius, 6 cm	$R_{\text{eff},6}$ ( $R_\odot$ )	560	410
effective radius, 20 cm	$R_{\text{eff},20}$ ( $R_\odot$ )	1300	950

**Notes.** Orbital parameters from Rauw (2013, pers. comm.), which is an updated version of the results published by Rauw et al. (2012). Radio data are determined from the Wright & Barlow (1975) equations.

stars will be far apart and we would therefore expect little effect of the stellar wind absorption. For a first estimate of the effect we can make use of the effective radii listed in Table 2: these give an indication of the extent of the radio photospheres. We see that for the shorter wavelengths, even at periastron (where the separation between the stars is  $\sim 1300 R_\odot$ ) the CWR is outside the radio photospheres of each of the stars. Therefore no significant absorption of the synchrotron photons occurs.

Away from periastron, the spectral index is nearly flat, or slightly negative. The fluxes at all wavelengths are of order 2 mJy, slightly lower at 2 cm and somewhat higher at 20 cm. This indicates that we are seeing the non-thermally emitting CWR during a large part of the orbit. It is therefore not completely hidden part of the time, as was the case during the periastron passage of Cyg OB2 # 9 (Blomme et al. 2013). As mentioned above, this can be attributed to the longer period of 9 Sgr, resulting in a CWR region that stays out of the free-free region of each star.

The contribution of the thermal free-free emission of the stellar winds of both stars is negligible. Using the equations of Wright & Barlow (1975) we can calculate the expected thermal radio flux, using the parameters listed in Table 2. The combined flux of both binary components is 0.02 mJy at 2 cm and 0.005 mJy at 20 cm, which is much smaller than the observed fluxes.

#### 4. Modelling

To model the radio-light curve, we basically use the same simple model as presented by Blomme et al. (2013). The use of such a simple model avoids the introduction of less well-known quantities, such as the shock strength, the local magnetic field and the efficiency of Fermi mechanism.

One of the simplifications in the model is that it assumes a simple shape for the CWR. This is more consistent with a CWR in the adiabatic regime than a radiative one where the instabilities create a lot of structure (Stevens et al. 1992; Pittard 2009). That the CWR of 9 Sgr stays in the adiabatic regime can be seen

by comparing the cooling time ( $t_{\text{cool}}$ ) to the escape time ( $t_{\text{esc}}$ ), using the equation from Stevens et al. (1992):

$$\chi = \frac{t_{\text{cool}}}{t_{\text{esc}}} \approx \frac{v_8^4 d_{12}}{M_{-7}}, \quad (1)$$

with  $v_8$  the wind velocity in units of  $1000 \text{ km s}^{-1}$ ,  $d_{12}$  the distance to the contact discontinuity in units of  $10^7 \text{ km}$  and  $M_{-7}$  the mass-loss rate in units of  $10^{-7} M_\odot \text{ yr}^{-1}$ . Using the values from Table 2 and assuming the contact discontinuity to be half-way between the two stars, we find  $\chi \approx 740 - 4700$ , where the range covers the difference between periastron and apastron values. The high  $\chi$  values indicate that the collision is indeed adiabatic (see also Rauw et al. 2012).

In the model, we solve the radiative transfer in a three-dimensional grid. For each phase in the orbit, we position the stars in this grid, taking into account the orbital parameters and the estimated inclination (Table 2). For a large part of the grid, the volume is filled with wind material coming from the closer-by star. This wind material will contribute to the radio flux through the free-free emission (but we expect the contribution to be small – see Sect. 3). The density at any point in the model is derived from the mass-loss rate and terminal velocity (Table 2). We caution that these two quantities are not well known. The spectral classification of both components is hampered by the fact that the He II lines cannot be well disentangled (Rauw et al. 2012). This classification is then used to determine the mass-loss rate and terminal velocity from the Martins et al. (2005) calibration. Furthermore, any given spectral type/luminosity class corresponds to a range of effective temperature and luminosity rather than the unique values given by the Martins et al. calibration (Weidner & Vink 2010). This turned out to be an important effect in our analysis of Cyg OB2 #9 (Blomme et al. 2013).

For material inside the CWR, we multiply the density by a factor of 4 to take into account the compression in the shocks. The wind material is assumed to be at  $T=20,000 \text{ K}$ , i.e. just below half of the effective temperature of the stars. A higher temperature is assigned to the material inside the CWR (see below). The grid is  $100,000 R_\odot$  on each side and is centred on the centre of gravity of the binary system.

For the shape of the CWR, we considered two options. The first one is as presented in Blomme et al. (2013): the region has the shape of a cone, rotationally symmetric around the line connecting the two stars. The position of this cone and its opening angle are derived from Eichler & Usov (1993, their Eqs. (1) and (3)). The cone is also given a finite thickness which remains constant in the whole simulation volume (Blomme et al., their Fig. 3). Hydrodynamical simulations of adiabatic wind collisions (e.g. Lamberts et al. 2011, their Fig. 4) show a somewhat different shape. In these calculations, the CWR is thin near the apex (on the line connecting the two stars) and flares out as we move away from that line. We therefore also considered a second option, where the cone has a “flaring” angle ( $\alpha$ ) instead of a finite thickness. (see Fig. 2). For both options, we limit the size of the CWR. Eichler & Usov (1993) estimate the size to be  $\pi$  times the distance from the apex to the weaker-wind star. In our model, we assume that the size (denoted  $R_{\text{CWR}}$ ) scales proportionally to the distance between the two stars ( $D$ ), with the scaling factor a free parameter.

Because the material inside the CWR is hot and compressed it will also contribute to the radio flux through free-free emission (Pittard 2010). We therefore need to assign a temperature to this hot material. Rauw et al. (2002) fit the X-ray emission of this system with a multi-temperature thermal model with

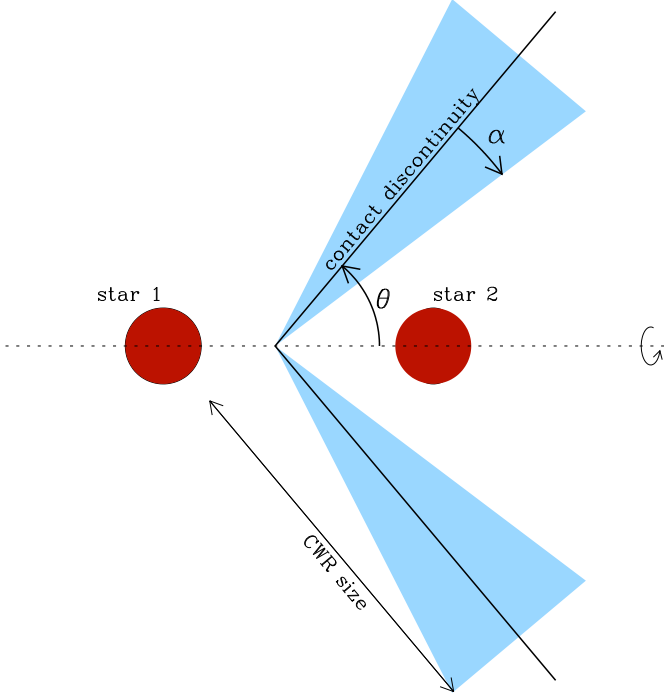


**Fig. 2.** Schematic view of the second option for our model for the CWR. At any given phase, the shape of the CWR (shaded in light-blue) is a cone that is rotationally symmetric around the axis connecting the two stars. It has a (half) opening angle  $\theta$ , a (half) flaring angle  $\alpha$  and a size ( $R_{\text{CWR}}$ ) which scales with the separation ( $D$ ) between the two components.

components at  $kT=0.25\text{--}0.26$  keV,  $0.67\text{--}0.73$  keV and possibly  $> 1, 46$  keV. This corresponds to temperatures of  $3 \times 10^6$ ,  $8 \times 10^6$ , and  $2 \times 10^7$  K respectively. In the models we typically run, we calculate the emission measure for the CWR material as:

$$\text{EM} = \int_{\text{CWR}} n_e n_H dV, \quad (2)$$

where  $n_e$  is the electron number density and  $n_H$  is the proton number density. The integration is over the whole volume of the CWR, and gives a range of values of  $\log \text{EM} \approx 55.2 - 57.2$  ( $\text{EM}$  in  $\text{cm}^{-3}$ ). The observed emission measures of the X-ray temperatures are respectively  $\log \text{EM} = 56.2, 55.5$  and  $54.7$ . This leads to an average temperature of the model CWR of  $2 \times 10^5 - 5 \times 10^6$  K. To simplify the model, we assign a single temperature of  $1.0 \times 10^6$  K to the hot CWR material. Because of the high ratio of the cooling time to the escape time, these temperatures will not significantly decrease inside the CWR as we move away from the apex.

We further assume that all the material in the CWR also emits synchrotron radiation. The amount emitted is described by its brightness temperature ( $T_{\text{sync}}$ ), which we consider as a free parameter in our model.

The radiative transfer equation is then solved in this 3D grid, following the procedure outlined in Wright & Barlow (1975). We take into account the free-free emission and absorption processes in the stellar winds and CWR, as well as the synchrotron emission in the CWR. Note that the synchrotron brightness temperature does not play a role in the absorption because synchrotron self-absorption has little effect at GHz frequencies

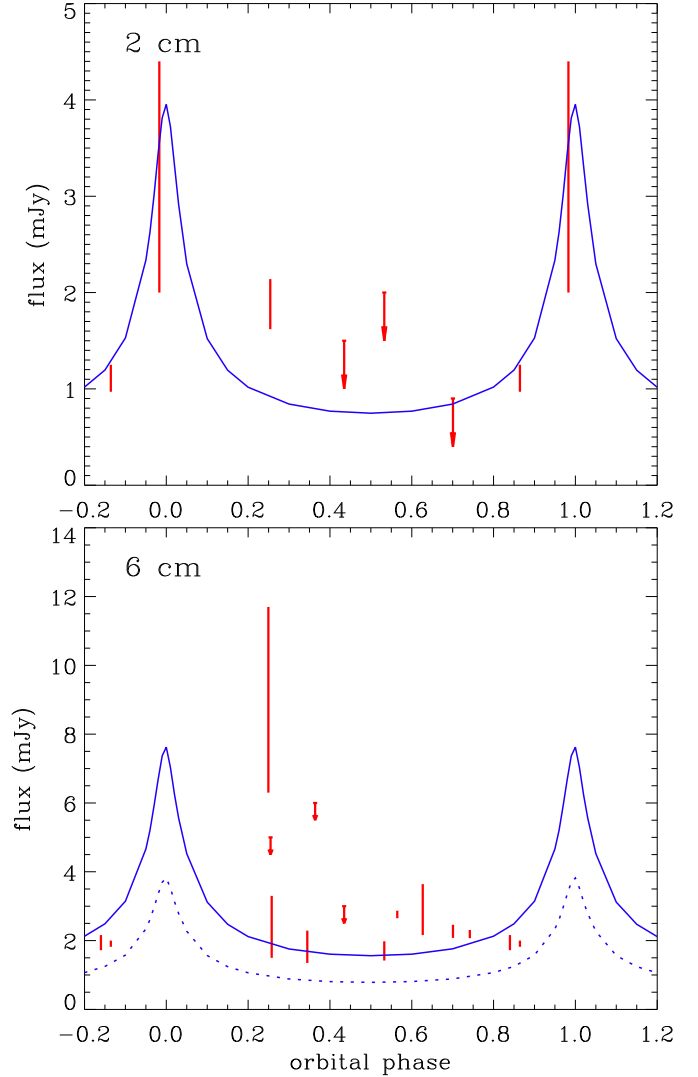


**Fig. 3.** Comparison between 9 Sgr observed and model radio fluxes, as a function of orbital phase in the 9.1-year period. Top: 2 cm fluxes, bottom: 6 cm fluxes. The observed data are plotted in red, the theoretical fluxes of the best-fit model in blue. In the bottom panel, the dotted blue line shows the best-fit 2-cm model applied to the 6-cm data.

(Pittard et al. 2006). We use an adaptive grid scheme, which refines the grid only in those places where needed to get the required precision in specific intensity and flux.

## 5. Results and discussion

We started by fitting the 2-cm radio light curve, because at this wavelength we see the clearest evidence of phase-locked variability (see Fig. 1). For the observed light curve we used the fluxes from the “combined” data (see Sect. 2) instead of the separate ones, because the combined data have a smaller error bar.

In the model calculations we tried both options for the shape of the CWR, but the more realistic one – where the thickness of the CWR increases as we move away from the apex – gives the better results. We explored the parameter space of the synchrotron brightness temperature ( $T_{\text{sync}}$ ), flaring angle ( $\alpha$ ) and size of the CWR ( $R_{\text{CWR}}$ ). Formally, the best-fit parameters are:

$T_{\text{sync}} = 4.0 \times 10^8$  K,  $\alpha = 40^\circ$ ,  $R_{\text{CWR}} = 2.0 D$ ; this solution is shown on Fig. 3 (top panel, blue solid line). The result is not very unique however. It is quite insensitive to the size of the CWR, and other combinations of  $T_{\text{sync}}$  and  $\alpha$  can give an almost equally good fit. Our calculations show that this is the case when the combination  $T_{\text{sync}}\alpha^{0.8}$  has the same value as our formal best fit. Values for the half-flaring angle larger than  $40^\circ$  were not explored, as this would make the size of the CWR hydrodynamically unlikely.

The agreement of the theoretical curve with the observed fluxes is good. We correctly predict an increase of the 2-cm flux around periastron (up to  $\sim 4$  mJy) and a roughly constant flux away from periastron (at the  $\sim 1$  mJy level). The only discrepant point is at phase 0.25. This indicates that the light curve around periastron is not as symmetric as suggested by the theoretical calculations: the higher flux level extends for a longer time after periastron passage than before it.

We explored the contribution of the various emission and absorption processes to this theoretical light curve by manipulating the temperature and density enhancement in the CWR. If we switch off the synchrotron emission and the density enhancement in the CWR, and set the CWR temperature equal to the wind temperature, we find the free-free contribution of the stellar winds. This turns out to be 0.020 mJy, in good agreement with the values listed in Table 2. By switching off only the synchrotron emission, we find the combined free-free contribution of the stellar winds and the CWR: this is 0.021–0.027 mJy (depending on orbital phase). The free-free emission of the CWR is therefore very small. Finally, switching off the free-free absorption in the stellar wind changes the fluxes by only a few percent. The 2-cm radio light curve in Fig. 3 is therefore almost exclusively due to synchrotron emission.

Free-free absorption in the CWR does play an important role, as can be seen from the following argument. An object with a brightness temperature  $T_{\text{sync}} = 4.0 \times 10^8$  K at a distance  $d = 1.79$  kpc with a size equal to the separation between the two components ( $D = 3011/\sin(45^\circ) R_\odot$ ) has a flux of

$$S_\nu = \pi \left( \frac{D}{d} \right)^2 \frac{2kT_{\text{sync}}}{\lambda^2} \approx 25\,000 \text{ mJy.} \quad (3)$$

This is clearly more than the 1–4 mJy from the model calculation, hence a large amount of the synchrotron flux must be absorbed in the CWR.

The model used here has a number of simplifying assumptions. One is that the synchrotron brightness temperature is the same for all phases in the orbit. The synchrotron emission is however proportional to the number of relativistic electrons (Rybicki & Lightman 1986, Chap. 6). We therefore also tried models with a synchrotron brightness temperature that is proportional to the local electron density (this assumes that the fraction of electrons that becomes relativistic is the same at all phases of the orbit). Such models result in a much higher contrast between the maximum and minimum flux, and are therefore not a good fit to the 2-cm observations.

We next applied the same model to the 6 cm fluxes. This is shown by the dotted blue line in the bottom panel of Fig. 3. The model clearly underestimates the observed fluxes. This is not surprising as the synchrotron brightness temperature need not be the same for 6 cm as for 2 cm. In a more detailed synchrotron emission model (such as used by Blomme et al. 2010) we would, in principle, be able to calculate the synchrotron brightness temperature for all wavelengths. We note however that the model of Blomme et al. was not able to explain the observed spectral in-

dex of Cyg OB2 #8A, a quantity which is directly related to the relative synchrotron brightness temperatures.

We therefore again considered the synchrotron brightness temperature as a free parameter and tried to fit the 6-cm observations. We kept the flaring angle and CWR size at their 2-cm best-fit values. The best-fit result is shown by the full blue line in Fig. 3 (bottom panel) and has a brightness temperature of  $T_{\text{sync}} = 8.0 \times 10^8$  K. Away from periastron we obtain the  $\sim 2$  mJy level, as observed. We have no 6-cm observations around periastron itself, so we cannot judge if the flux maximum has the correct value. The most discrepant point in the fit is what happens around phase 0.25: there we have two observations which are seemingly in contradiction: one at  $9.0 \pm 2.7$  mJy and one at  $2.4 \pm 0.9$  mJy. These flux determinations do not suffer from the measurement problems due to the nearby Hourglass Nebula (Sect. 2). They were taken in VLA configurations that have medium to high spatial resolution, where the effect of the Hourglass Nebula is small. We note however that both have large error bars, so these detection are only at the  $\sim 3\sigma$  level. As for the 2-cm light curve, the parameters are not well determined and other combinations give fits of a similar quality.

9 Sgr is exceptional among the O-type non-thermal radio emitters in that it is the one with the longest period among those that have their spectroscopic orbit determined. Cyg OB2 #8A has a substantially shorter period (21.9 d). While one might expect that in such a short-period binary all synchrotron emission would be absorbed by the stellar winds, it turns out that this is still a non-thermal radio emitter (De Becker et al. 2004; Blomme et al. 2010). HD 168112 ( $P = 1.4?$  yr, Blomme et al. 2005) and Cyg OB2 #9 ( $P = 2.35$  yr, Nazé et al. 2008; Van Loo et al. 2008; Nazé et al. 2012; Blomme et al. 2013) are longer-period binaries with clear non-thermal emission. For Cyg OB2 #9 we know that the CWR is radiative at least during some part of the orbit. This complicates the modelling of the emission. Furthermore, with these periods, the effect of orbital motion that turns the CWR into a spiral shape, will be important (e.g. Pittard 2009).

There are other O-type non-thermal radio emitters that have longer periods. Cyg OB2 #5 is a 6.6-d spectroscopic binary, but the 6.7-yr period in the radio fluxes indicates the presence of a third companion. Furthermore, a CWR is visible at radio wavelengths between Cyg OB2 #5 and a nearby B-type star, implying that Cyg OB2 #5 could be a quadruple system (Kennedy et al. 2010; Dzib et al. 2013). From spectroscopy we know that HD 167971 is a 3.3-d binary, with a third component which may or may not be gravitationally bound (Leitherer et al. 1987). Radio data do not show the 3.3-d period, but reveal a period of  $\sim 20$  yr, or longer, suggesting that this is due to the CWR between the binary and the third component (Blomme et al. 2007).

What makes 9 Sgr an excellent candidate for modelling studies is that it has an adiabatic wind collision and that it is much less influenced by orbital motion. Longer-period systems (such as Cyg OB2 #5 and HD 167971) might be even better, but they lack the spectroscopic orbital information. A disadvantage of 9 Sgr is that the radio coverage of the orbit, especially at periastron, is somewhat lacking. It should however be easy to remedy that situation thanks to the recent upgrade of radio telescopes such as the Karl G. Jansky Very Large Array (JVLA).

## 6. Conclusions

Using archive data from the VLA that cover a time range of 24 years, we determined the radio light curve of the massive O-type binary 9 Sgr. The presence of the nearby Hourglass Nebula, a strong radio source, seriously hampers the detection of 9 Sgr

when the VLA is in one of its configurations with lower spatial resolution. The quality of the radio light curve is therefore less than that of other systems studied in this series of papers.

Notwithstanding these problems, the 2-cm light curve shows clear phase-locked variability with the 9.1-yr orbit of this system. Fluxes are higher around periastron, as expected, because in this highly eccentric system the wind-wind collision is much stronger (i.e. has a higher ram pressure) when the stars are closer to each other. The 6 cm light curve seems to follow a similar trend, although observations at the periastron passage are missing. The few data we have at 20 cm are more puzzling, as they seem to show large variations at other phases than periastron. The spectral index is approximately zero, and even outside the periastron phases the fluxes are so high that almost all of the emission can be ascribed to synchrotron radiation in the colliding-wind region (CWR).

A simple model provides a good fit to the 2-cm observations, and allows us to estimate that the synchrotron brightness temperature of the CWR is at least  $4 \times 10^8$  K. Higher values of the brightness temperature are also possible, provided the flaring angle is smaller. The geometric extent of the CWR is not well constrained in this fitting procedure. We caution that this simple model lacks many important ingredients, such as the hydrodynamics of the CWR, the efficiency with which the electrons get accelerated up to relativistic speeds, the local magnetic field and the quenching due to the Razin effect.

We propose that 9 Sgr is an ideal candidate for more detailed modelling of its radio emission. Its orbital parameters are sufficiently well known. It has a long period and because of the larger distance between the two components the collision region remains adiabatic during the whole orbit. Also, the effect of orbital motion on the shape of the CWR is much smaller than in other binary systems. All this simplifies the hydrodynamical part of the modelling. Observationally, the coverage of the orbit should be improved, especially around periastron. This should be quite feasible using recently upgraded radio telescopes such as the JVLA.

*Acknowledgements.* We thank Gregor Rauw for providing updated values for the orbital parameters and Joan Vandekerckhove for his help with the reduction of the VLA data. We are grateful to the original observers of the VLA archive data used in this paper. D. Volpi acknowledges funding by the Belgian Federal Science Policy Office (Belspo), under contract MO/33/024. This research has made use of the SIMBAD database, operated at CDS, Strasbourg, France and NASA's Astrophysics Data System Abstract Service.

## References

- Abbott D.C., Biegging J.H., Churchwell E., Cassinelli J.P., May 1980, ApJ, 238, 196  
 Abbott D.C., Biegging J.H., Churchwell E., Nov. 1981, ApJ, 250, 645  
 Abbott D.C., Biegging J.H., Churchwell E., May 1984, ApJ, 280, 671  
 Biegging J.H., Abbott D.C., Churchwell E.B., May 1989, ApJ, 340, 518  
 Blomme R., Van Loo S., De Becker M., et al., Jun. 2005, A&A, 436, 1033  
 Blomme R., De Becker M., Runacres M.C., van Loo S., Setia Gunawan D.Y.A., Mar. 2007, A&A, 464, 701  
 Blomme R., De Becker M., Volpi D., Rauw G., Sep. 2010, A&A, 519, A111  
 Blomme R., Nazé Y., Volpi D., et al., Feb. 2013, A&A, 550, A90  
 Bridle A.H., Schwab F.R., 1999, In: Taylor G.B., Carilli C.L., Perley R.A. (eds.) Synthesis Imaging in Radio Astronomy II, vol. 180 of Astronomical Society of the Pacific Conference Series, 371  
 De Becker M., Rauw G., Manfroid J., Sep. 2004, A&A, 424, L39  
 Dworetzky M.M., Jun. 1983, MNRAS, 203, 917  
 Dzib S.A., Rodríguez L.F., Loinard L., et al., Feb. 2013, ApJ, 763, 139  
 Eichler D., Usov V., Jan. 1993, ApJ, 402, 271  
 Gagné M., Fehon G., Savoy M.R., et al., Dec. 2012, In: Drissen L., Rubert C., St-Louis N., Moffat A.F.J. (eds.) Proceedings of a Scientific Meeting in Honor of Anthony F. J. Moffat, vol. 465 of Astronomical Society of the Pacific Conference Series, 301

- Kennedy M., Dougherty S.M., Fink A., Williams P.M., Feb. 2010, ApJ, 709, 632  
 Kumar D.L., Anandarao B.G., Sep. 2010, MNRAS, 407, 1170  
 Lamberts A., Fromang S., Dubus G., Dec. 2011, MNRAS, 418, 2618  
 Leitherer C., Forbes D., Gilmore A.C., et al., Oct. 1987, A&A, 185, 121  
 Martins F., Schaerer D., Hillier D.J., Jun. 2005, A&A, 436, 1049  
 Nazé Y., De Becker M., Rauw G., Barbieri C., May 2008, A&A, 483, 543  
 Nazé Y., Mahy L., Damerdjij Y., et al., Oct. 2012, A&A, 546, A37  
 Perley R., Taylor G., 2003, VLA Calibrator Manual (<http://www.vla.nrao.edu/astro/calib/manual/index.shtml>)  
 Pittard J.M., Jul. 2009, MNRAS, 396, 1743  
 Pittard J.M., Apr. 2010, MNRAS, 403, 1633  
 Pittard J.M., Dougherty S.M., Coker R.F., O'Connor E., Bolingbroke N.J., Feb. 2006, A&A, 446, 1001  
 Rauw G., Blomme R., Waldron W.L., et al., Nov. 2002, A&A, 394, 993  
 Rauw G., Sana H., Gosset E., et al., Nov. 2005, In: Rauw G., Nazé Y., Blomme R., Gosset E. (eds.) Massive Stars and High-Energy Emission in OB Associations, 85  
 Rauw G., Sana H., Spano M., et al., Jun. 2012, A&A, 542, A95  
 Rybicki G.B., Lightman A.P., Jun. 1986, Radiative Processes in Astrophysics (New York, Wiley-Interscience)  
 Stevens I.R., Blondin J.M., Pollock A.M.T., Feb. 1992, ApJ, 386, 265  
 Van Loo S., Runacres M.C., Blomme R., Jun. 2006, A&A, 452, 1011  
 Van Loo S., Blomme R., Dougherty S.M., Runacres M.C., May 2008, A&A, 483, 585  
 Weidner C., Vink J.S., Dec. 2010, A&A, 524, A98  
 White R.L., Feb. 1985, ApJ, 289, 698  
 Wright A.E., Barlow M.J., Jan. 1975, MNRAS, 170, 41

**Appendix A: Data table**



**Table A.1.** 9 Sgr VLA data.

(1)	(2)	(3)	(4)	(5)	(6)	(7)	(8)	(9)	(10)
Progr.	Date	Ctr.	Phase Calibrator		Dist.	Int.	No.	Config.	Flux
			Name	Flux (Jy)					
					(degr.)	Time (min)	Ants.		(mJy)
<b>0.7 cm</b>									
AR328	1995-04-27	9 Sgr	1733-130	10.67 ± 0.08	13.4	17	9	D	< 25.
<b>2 cm</b>									
BIEG	1982-02-09	9 Sgr	1733-130	4.17 ± 0.05	13.4	103	23	AD	< 2.
AC42	1983-08-22	9 Sgr	1733-130	5.91 ± 0.10	13.4	47	23	A	< 0.9
AB327	1985-01-28	9 Sgr	1733-130	6.99 ± 0.14	13.4	30	26	A	1.46 ± 0.30
AC116	1985-02-16	9 Sgr	1733-130	6.46 ± 0.04	13.4	37	24	A	1.01 ± 0.28
<i>combined AB327+AC116</i>									1.11 ± 0.14
AT89	1988-01-22	M8	1733-130	5.16 ± 0.03	13.4	105	25	B	< 15.
AH265	1988-05-05	M8UU1	1733-130	4.92 ± 0.08	13.4	40	22	CD	< 50.
AR328	1995-04-27	9 Sgr	1733-130	9.74 ± 0.03	13.4	22	15	D	(3.2 ± 1.2)
AH557	1996-01-23	M8	1733-130	11.10 ± 0.05	13.4	33	26	CnB	< 50.
AW478	1997-10-03	9 Sgr	1744-312	0.751 ± 0.007	8.1	13	22	DnC	< 16.
AW478	1997-10-07	9 Sgr	1744-312	0.788 ± 0.002	8.1	13	25	DnC	2.6 ± 0.9
AW478	1997-10-11	9 Sgr	1744-312	0.790 ± 0.007	8.1	13	25	DnC	< 4.
AW478	1997-10-15	9 Sgr	1744-312	0.844 ± 0.003	8.1	13	26	DnC	< 2.
<i>combined AW478</i>									1.88 ± 0.26
AW515	1999-06-08	9 Sgr	1820-254	0.896 ± 0.003	4.0	30	18	AD	< 1.5
<b>3.6 cm</b>									
AW304	1992-01-24	9 Sgr	1924-292	17.13 ± 0.78	18.7	11	24	CnB	< 9.
AB671	1993-01-21	9 Sgr	1811-209	0.1684 ± 0.0007	3.8	19	22	A	1.59 ± 0.09
AB671	1993-01-24	9 Sgr	1811-209	0.1709 ± 0.0005	3.8	19	26	A	1.41 ± 0.13
AB671	1993-01-29	9 Sgr	1811-209	0.1713 ± 0.0004	3.8	19	25	BnA	1.71 ± 0.26
AB671	1993-02-01	9 Sgr	1811-209	0.1699 ± 0.0006	3.8	13	26	BnA	1.33 ± 0.18
AB671	1993-02-14	9 Sgr	1811-209	0.1745 ± 0.0004	3.8	9	26	BnA	1.80 ± 0.30
<i>combined AB671</i>									1.36 ± 0.06
AR328	1995-04-27	9 Sgr	1733-130	6.74 ± 0.02	13.4	11	15	D	< 6.
AH557	1995-09-25	M8	1733-130	7.879 ± 0.015	13.4	28	26	BnA	3.72 ± 0.44
AW478	1997-10-03	9 Sgr	1751-253	0.2579 ± 0.0008	2.9	13	26	DnC	< 3.
AW478	1997-10-07	9 Sgr	1751-253	0.2724 ± 0.0003	2.9	13	26	DnC	< 2.
AW478	1997-10-11	9 Sgr	1751-253	0.2665 ± 0.0006	2.9	13	26	DnC	< 4.
AW478	1997-10-15	9 Sgr	1751-253	0.2698 ± 0.0004	2.9	13	26	DnC	< 90.
AW478	1997-10-18	9 Sgr	1751-253	0.2710 ± 0.0005	2.9	9	25	DnC	3.8 ± 1.3
<i>combined AW478</i>									1.78 ± 0.36
AB1005	2001-03-08	9 Sgr	1751-253	0.2658 ± 0.0015	2.9	8	25	B	3.6 ± 0.9
AW574	2002-03-29	[1]	1751-253	0.2705 ± 0.0005	2.9	2	25	A	< 5.
AK559	2003-04-05	G9.97	1820-254	0.6580 ± 0.0008	4.1	15	25	D	< 20.
AF399	2003-06-07	[2]	1820-254	0.636 ± 0.002	4.0	21	27	A	1.81 ± 0.08
AB1094	2003-07-05	18006	1820-254	0.7611 ± 0.0012	4.1	20	26	A	2.3 ± 0.55
AF399	2003-09-09	[2]	1820-254	0.6825 ± 0.0019	4.0	21	27	A	1.85 ± 0.17
<b>6 cm</b>									
CHUR	1979-07-13	9 Sgr	1733-130	5.38 ± 0.10	13.4	186	13	AC	9.0 ± 2.7
NEWE	1979-08-07	9 Sgr	1733-130	5.64 ± 0.13	13.4	112	14	AC	(5.2 ± 2.4)
NEWE	1979-08-09	9 Sgr	1733-130	5.38 ± 0.10	13.4	30	14	AC	< 20.
<i>combined NEWE</i>									(2.4 ± 0.9)
CHUR	1980-05-23	9 Sgr	1733-130	4.60 ± 0.10	13.4	30	21	AC	< 4.
CHUR	1980-05-24	9 Sgr	1733-130	5.40 ± 0.02	13.4	49	22	AC	1.88 ± 0.40
<i>combined CHUR</i>									1.82 ± 0.47
BIEG	1980-07-26	9 Sgr	1733-130	5.242 ± 0.015	13.4	10	20	C	< 8.
BIEG	1980-07-27	9 Sgr	1733-130	5.187 ± 0.017	13.4	19	20	C	< 11.
<i>combined BIEG</i>									< 6.
SIMO	1980-09-08	Her 36	1911-201	2.51 ± 0.03	16.2	0	23	D	< 9.
BROW	1981-12-28	G5.973	1751-253	0.532 ± 0.002	2.9	6	26	C	< 9.

**Table A.1.** continued.

(1) Progr.	(2) Date	(3) Ctr.	(4)		(5) Phase Calibrator Flux (Jy)	(6) Dist. (degr.)	(7) Int. Time (min)	(8) No. Ants.	(9) Config.	(10) Flux (mJy)
			Name							
BIEG	1982-02-09	9 Sgr	1733-130		$4.82 \pm 0.04$	13.4	19	23	AC	$1.70 \pm 0.28$
BIGN	1982-05-26	9 Sgr	1733-130		$5.090 \pm 0.013$	13.4	34	25	A	$2.76 \pm 0.11$
BROW	1982-11-12	G5.973	1751-253		$0.534 \pm 0.004$	2.9	6	26	D	< 25.
AH11	1983-02-06	M8	1911-201		$2.668 \pm 0.015$	16.2	50	25	C	< 9.
AJ97	1983-08-19	9 Sgr	1733-130		$5.47 \pm 0.18$	13.4	55	25	A	$2.35 \pm 0.32$
AC42	1983-08-22	9 Sgr	1733-130		$5.090 \pm 0.015$	13.4	32	24	A	$2.20 \pm 0.14$
<i>combined AJ97+AC42</i>										
AC116	1984-11-27	9 Sgr	1733-130		$4.978 \pm 0.006$	13.4	9	24	A	$1.94 \pm 0.22$
AB327	1985-01-28	9 Sgr	1733-130		$5.117 \pm 0.015$	13.4	17	26	A	$2.08 \pm 0.19$
AC116	1985-02-16	9 Sgr	1733-130		$5.266 \pm 0.006$	13.4	19	24	A	$1.96 \pm 0.13$
<i>combined AB327+AC116</i>										
AG178	1985-04-08	M8CO1	1751-253		$0.4826 \pm 0.0007$	2.9	63	25	BnA	< 1.6
AW158	1986-04-27	G5.97M8	1811-209		$0.3081 \pm 0.0006$	3.9	4	24	A	$10.3 \pm 1.5$
AH259	1987-02-01	M8	1733-130		$6.24 \pm 0.02$	13.4	162	24	DnC	< 6.
AH265	1987-04-24	M8CC1	1733-130		$6.580 \pm 0.017$	13.4	50	26	D	< 8.
AT89	1988-01-22	M8	1733-130		$5.914 \pm 0.010$	13.4	62	25	B	$3.9 \pm 0.63$
AH265	1988-05-05	M8CC1	1751-253		$0.474 \pm 0.002$	2.9	38	23	C	< 7.
AB671	1993-01-21	9 Sgr	1811-209		$0.3093 \pm 0.0009$	3.8	19	24	A	$2.36 \pm 0.15$
AB671	1993-01-24	9 Sgr	1811-209		$0.3142 \pm 0.0009$	3.8	19	26	A	$2.34 \pm 0.28$
AB671	1993-01-29	9 Sgr	1811-209		$0.3179 \pm 0.0004$	3.8	19	25	BnA	$2.17 \pm 0.46$
AB671	1993-02-01	9 Sgr	1811-209		$0.3140 \pm 0.0004$	3.8	12	25	BnA	$2.13 \pm 0.24$
AB671	1993-02-14	9 Sgr	1811-209		$0.3159 \pm 0.0005$	3.8	10	25	BnA	< 20.
<i>combined AB671</i>										
AR328	1995-04-27	9 Sgr	1733-130		$5.049 \pm 0.015$	13.4	11	15	D	< 30.
AH557	1995-09-26	M8	1733-130		$5.470 \pm 0.005$	13.4	33	26	BnA	$3.4 \pm 0.9$
AW478	1997-10-03	9 Sgr	1751-253		$0.4773 \pm 0.0008$	2.9	13	26	DnC	< 9.
AW478	1997-10-07	9 Sgr	1751-253		$0.4778 \pm 0.0011$	2.9	13	26	DnC	< 7.
AW478	1997-10-11	9 Sgr	1751-253		$0.4792 \pm 0.0006$	2.9	13	26	DnC	< 6.
AW478	1997-10-15	9 Sgr	1751-253		$0.4773 \pm 0.0005$	2.9	13	26	DnC	< 6.
AW478	1997-10-18	9 Sgr	1751-253		$0.4766 \pm 0.0014$	2.9	8	24	DnC	< 6.
<i>combined AW478</i>										
AW515	1999-06-08	9 Sgr	1820-254		$0.9992 \pm 0.0016$	4.0	10	25	AD	< 3.
AB1005	2001-03-08	9 Sgr	1751-253		$0.4495 \pm 0.0009$	2.9	8	25	B	$2.9 \pm 0.74$
AB1094	2003-07-05	18006	1820-254		$0.695 \pm 0.002$	4.1	20	26	A	$(7.1 \pm 3.7)$
<b>20 cm</b>										
BIGN	1982-05-26	9 Sgr	1733-130		$5.38 \pm 0.02$	13.4	72	25	A	$5.23 \pm 0.20$
AC42	1983-08-22	9 Sgr	1733-130		$4.525 \pm 0.015$	13.4	31	25	A	$3.24 \pm 0.37$
AG163	1984-12-07	022	1751-253		$1.069 \pm 0.008$	3.0	1	22	A	< 25.
AC116	1984-12-21	9 Sgr	1733-130		$5.86 \pm 0.02$	13.4	10	26	A	< 25.
AR120	1985-01-24	G6.0	1811-209		$0.893 \pm 0.010$	3.9	13	25	A	< 60.
AR120	1985-01-26	G6.0	1811-209		$0.879 \pm 0.004$	3.9	9	26	A	< 50.
<i>combined AR120</i>										
AR283	1993-01-10	G006-5	1751-253		$0.980 \pm 0.005$	3.1	12	26	A	< 50.
AT143	1993-02-20	0060-010	1751-253		$1.041 \pm 0.008$	2.8	4	26	BnA	< 30.
AR359	1996-08-29	M8E	1733-130		$5.367 \pm 0.011$	13.6	6	26	D	< 35.
AY76	1996-11-23	M8E	1751-253		$1.033 \pm 0.003$	3.1	4	26	A	< 25.
AB1005	2001-03-08	9 Sgr	1751-253		$1.177 \pm 0.002$	2.9	8	25	B	$12.7 \pm 3.6$
<b>90 cm</b>										
AJ194	1990-08-01	NGC6544	1830-360		$29.80 \pm 0.16$	12.2	90	25	B	< 50.

**Notes.** Column (1) gives the programme name, (2) the date of the observation, (3) the source on which the observation was centred, (4) the phase calibrator name (J2000 coordinates), (5) the phase calibrator flux and (6) the distance of the phase calibrator to the observed target, (7) the integration time on the source, (8) the number of antennas that gave a usable signal, (9) the configuration the VLA was in at the time of the observation, and (10) the measured flux. Upper limits are  $3 \times$  the RMS, values between brackets indicate marginal detections (signal-to-noise ratio < 3).

Abbreviations used in column (3) are: [1] = J1803-244; [2] = 18039-24216.